

Deep learning in the abyss: a stratified Physics Informed Neural Network for data assimilation

Vadim Limousin¹, Nelly Pustelnik¹, Bruno Deremble² and Antoine Venaille¹.

¹CNRS, ENS de Lyon, LPENSL, UMR5672, 69342, Lyon cedex 07, France

²Université Grenoble Alpes, CNRS, INRAE, IRD, Grenoble-INP, Institut des Géosciences de l'Environnement, Grenoble, France

Key Points:

- We propose a multi-layer Physics Informed Neural Networks suited for deep flow reconstruction.
- We demonstrate the potential of this method for data assimilation using SWOT-like and ARGO-like pseudo-observations in a three-layer quasi-geostrophic model.

arXiv:2503.19160v1 [physics.ao-ph] 24 Mar 2025

Corresponding author: Antoine Venaille, antoine.venaille@ens-lyon.fr

Corresponding author: Nelly Pustelnik, nelly.pustelnik@ens-lyon.fr

Abstract

The reconstruction of deep ocean currents is a major challenge in data assimilation due to the scarcity of interior data. In this work, we present a proof of concept for deep ocean flow reconstruction using a Physics-Informed Neural Network (PINN), a machine learning approach that offers an alternative to traditional data assimilation methods. We introduce an efficient algorithm called **StrAss-PINN** (for Stratified Assimilation PINNs), which assigns a separate network to each layer of the ocean model while allowing them to interact during training. The neural network takes spatiotemporal coordinates as input and predicts the velocity field at those points. Using a SIREN architecture (a multilayer perceptron with sine activation functions), which has proven effective in various contexts, the network is trained using both available observational data and dynamical priors enforced at several collocation points. We apply this method to pseudo-observed ocean data generated from a 3-layer quasi-geostrophic model, where the pseudo-observations include surface-level data akin to SWOT observations of sea surface height, interior data similar to ARGO floats, and a limited number of deep ARGO-like measurements in the lower layers. Our approach successfully reconstructs ocean flows in both the interior and surface layers, demonstrating a strong ability to resolve key ocean mesoscale features, including vortex rings, eastward jets associated with potential vorticity fronts, and smoother Rossby waves. This work serves as a prelude to applying **StrAss-PINN** to real-world observational data.

Plain Language Summary

Although bottom ocean currents are crucial for understanding overall ocean circulation, observations in the depths are limited, relying mainly on a few temperature, salinity, and pressure measurements. In contrast, the ocean’s surface is monitored in high detail by satellites. This article proposes using both the dynamical equations that describe vertical flow structure and advanced machine learning methods to reconstruct the full ocean dynamics. Since surface and bottom ocean dynamics are correlated, combining physical constraints with statistical analysis can help infer the entire system’s dynamics. This approach, called Physics-Informed Neural Networks (PINNs), integrates physics and statistical tools into a unified learning architecture.

1 Introduction

While satellites provide a vast amount of data on surface ocean currents (Fu et al., 1994; Fu et al, 2024), the interior remains sparsely observed, due to extreme conditions. Instruments such as localized moorings, ARGO floats (Wong et al., 2020), and acoustic measurements (Munk et al., 1995) offer valuable insights into deep layers, but reconstructing deep ocean dynamics from such limited data remains a major challenge. Reconstructing deep ocean currents is of tremendous importance, as deep flows play a central role in heat storage, carbon sequestration, and the oceanic energy budget (Fox-Kemper et al., 2021).

From a methodological point of view, the uneven distribution of data makes this inverse problem particularly difficult. Traditionally, this issue has been addressed using either statistical methods, e.g. (Guinehut et al., 2012), which are agnostic to the underlying flow model, or data assimilation techniques, which combine available data with a flow model to provide reanalysis (Blayo et al., 2014; Carrassi et al., 2018). Over the past decade, there has been a growing shift toward machine learning techniques (Sonnewald et al., 2021). In this paper, we focus on one of these methods — Physics-Informed Neural Networks (PINNs) (Karniadakis et al., 2021) — which can be considered as a machine learning counterpart to data assimilation. A key advantage of this approach is that the field to recover is encoded directly in the neural network, eliminating the need for a grid-based discretization of the field. However, a major challenge remains to train the network to reconstruct multiscale, chaotic flows — characteristics that are prevalent in ocean dynamics. Here, we develop a multilayer PINNs learning strategy called **StrAss-PINN**, for Stratified Assimilation PINNs.

We demonstrate its feasibility and utility for deep flow reconstruction. This is achieved in the presence of surface-intensified data and sparse subsurface data.

State-of-the-art on surface fields recovery – A large body of studies have been focused on reconstructing surface and subsurface fields from these data. For instance, regarding sea surface height (SSH) fields obtained from satellite altimeters, existing gridded datasets are produced using optimal interpolation (Ballarotta et al., 2019). Spatial resolution of the reconstructions can be improved using simple assimilation methods, such as nudging with simple and fast dynamical models (Le Guillou et al., 2021), or deep learning strategies with convolutional networks (Manucharyan et al., 2021). More recently, powerful data-driven techniques such as 4DVarNet have replaced the dynamical constraints in the assimilation variational problems with a penalty term involving a neural network in order to learn the dynamic from data themselves (Beauchamp et al., 2023). Other data-driven methods, decompositions into empirical orthogonal functions or autoencoders (Barth et al., 2020), have been used to reconstruct sea surface temperature (SST) fields in the presence of clouds that leads to spatio-temporal gaps in the data set. Learning efficient interpolation from both SST and SSH has also been addressed within various machine learning frameworks, e.g. (Martin et al., 2023; Fablet et al., 2024; Archambault et al., 2024).

Towards the recovery of deep ocean – The common feature of all the techniques mentioned above is the reconstruction of a 2d+t field. Data-driven methods have also been developed for 3d+t fields, provided there is sufficient data for at least some period of time. For example, Guinehut et al. (2012) used optimal interpolation and multilinear regression on climatological data to infer the vertical structure of mesoscale turbulence from observations alone. Similarly, Oulhen et al. (2024) combined data reduction techniques based on Empirical Orthogonal Functions (EOF) and analogs to reconstruct 3d+t temperature fields in the ocean’s upper layers, leveraging the ARGO dataset to learn statistical properties and reconstruct past fields from before the ARGO era. While promising, these methods are not ideal for reconstructing fields in regions that have never been intensively sampled, as statistical inference may not be reliable in such areas. For instance, trapped flow over seamounts may not always exhibit a clear signature at the surface (Venaille, 2012; G. C. Johnson & King, 2023). While moorings or deep ARGO floats provide useful local information on deep flows, global maps of deep ocean circulation can only be inferred using data assimilation techniques that combine data with flow models (Blayo et al., 2014). This approach has provided unvaluable reanalysis datasets, even if some unexpected behavior is also reported in some regions, see e.g. Lellouche et al. (2021). While successful for operational purposes, assimilation methods such as 4DVAR or the Ensemble Kalman Filter are often difficult to implement and computationally expensive. On the other hand, SSH interpolation via Deep Learning have been proven skillful to reconstructing subsurface mesoscale structures (Manucharyan et al., 2021). In all those cases, combining data from observations with dynamical constraints or deep learning approaches typically requires the introduction of a spatial grid, which incurs a significant computational cost as the spatio-temporal resolution increases. This highlights the need for more flexible methods that can incorporate dynamical constraints within a mesh-free framework. This is precisely where PINNs offer potentially an advantage.

PINNs, a grid-free assimilation technique – In a PINN, the physical state of the system (such as current velocity and density) is represented as the output of a neural network, while the input consists solely of spatio-temporal variables. The specificity of PINNs training is to ensure that the solution generated by the trained neural network not only satisfies the observed data but also adheres to the differential equations that describe the system’s dynamics. This is achieved by designing a training loss function composed of a data fidelity term, which ensures consistency with the observed data, and a penalty term, which quantifies the discrepancy between the network output and the assumed physical dynamics. The use of PINNs provides a threefold benefit: it bypasses the need to specify artificial boundary conditions when constructing the field in a given region, it is mesh free, avoiding thus the

need for discretization choices for the estimated field, and it provides useful flexibility in the choice of flow models, which can be adapted from case to case.

Following the original proposal (Raissi et al., 2019), PINNs have been applied to a wide range of fluid mechanics problems, from Rayleigh-Bénard convection (Lucor et al., 2022; Clark Di Leoni et al., 2023) to denoising measurements in stratified turbulence (Zhu et al., 2024), among a vast number of other examples (Karniadakis et al., 2021). Yet, applications of PINNs in atmospheric or oceanic field reconstruction are still in the early stages, see e.g. (Millet et al., 2023; Yoon et al., 2024). Notably, (Bang et al., 2024) addressed recently the ability of PINNs to reconstruct surface velocity field from surface drifter data. Implementing the PINN method in a realistic context such as mesoscale ocean turbulence (from 30 to 300km) presents several challenges, especially when multiple temporal and spatial scale are involved. Indeed, training these networks involves a delicate balance between ensuring data fidelity and adhering to physical laws, which can complicate the optimization process and lead to convergence issues, requiring the use of specialized techniques and strategies (Karniadakis et al., 2021).

Contributions – In the present work, we investigate the potential of PINNs to reconstruct deep ocean flows by leveraging minimal surface observations and sparse data from intermediate depths. Compared to state-of-the-art PINNs learning techniques, the proposed approach introduces a novel learning strategy by incorporating a multilayer training specifically tailored to multilayered ocean models. We demonstrate that the proposed PINNs can propagate information between vertical layers, reconstructing three-dimensional flow dynamics even with limited direct measurements from the deep ocean layer.

To evaluate the performance of the proposed **StrAss-PINN**, we consider a simplified wind-driven three-layer ocean model, a minimal yet representative framework for ocean dynamics. The upper layer is observed through surface data (similar to SWOT-like altimetry observations), while the interior and deep layers are observed by sparse point measurements (similar to ARGO floats), as sketched in Fig. 1. By integrating these observations with the known system dynamics, we show that PINNs can successfully reconstruct deep ocean flow, even with minimal data. This work serves as a proof of concept for the use of PINNs in ocean flow reconstruction, particularly in regions where data are sparse or indirect. Although this study does not directly compare our method with traditional assimilation techniques, it lays the groundwork for future research to refine and optimize this approach for real-world oceanographic applications.

2 State of the art and context

2.1 Data Assimilation

Data assimilation is a particular case of inverse problems. One has access to measurements of a signal altered by exterior known or unknown factors, such as noise, motion blur or, most notably in our case, the inability to observe the entire domain. For example, in the problem addressed in this work, observations are obtained from satellites and buoys, leading to partial sea surface data due to satellite coverage patterns and limited subsurface information resulting from the sparse data provided by buoys.

The typical approach to assimilation is a grid-based approach that can be framed as a minimization problem, where the cost function consists of two terms: a data fidelity term and a penalty that enforces predefined dynamics. The solution to the assimilation problem corresponds to the minimiser of this cost function. Formally, the goal is to recover the temporal sequence of 3d states $u(t, x, y, z)$, with each component of u representing different variables (e.g., pressure, velocity, temperature), and (t, x, y, z) indicating spatio-temporal locations on a grid of size $N = N_t \times N_x \times N_y \times N_z$. Assuming partial observations of the system at M distinct spatio-temporal points (represented by the vector d of size M), the

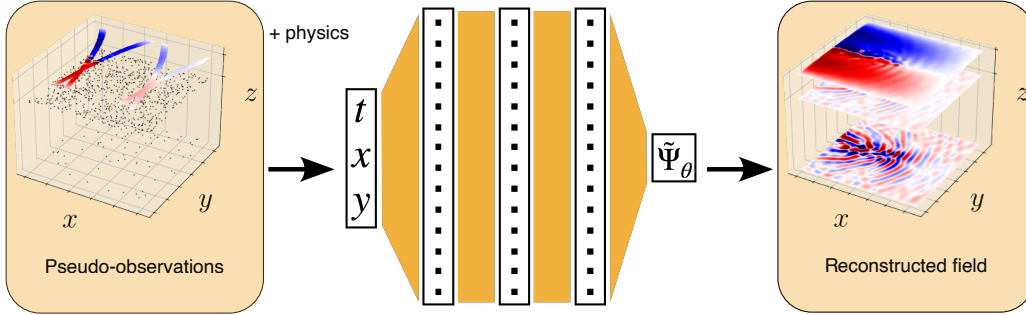


Figure 1: Schematic view of our method. Available (pseudo-)observations are provided by satellites for the surface and buoys in the ocean interior. They constitute the training set the networks aims to fit. This way, our method assimilates them additionally using explicit dynamics information through a physics-informed formalism to produce reasonable reconstructed fields. Finally, the networks are evaluated on a grid covering the domain, producing the reconstructed fields.

cost function to be minimized is defined as:

$$\mathcal{L}_{\text{DA}}(\mathbf{u}) = \|\mathcal{H}(\mathbf{u}) - \mathbf{d}\| + \|\mathcal{D}(\mathbf{u})\| \quad (1)$$

where \mathcal{H} represents the observation operator, which establishes the relationship between the complete quantity to be recovered of size N and the grid locations where observations are available. Additionally, \mathcal{D} represents the physical model. The first term is referred to as the data term and ensures the reconstructed field matches the observed data \mathbf{d} as well as possible. The second term is the dynamic information and ensures the reconstructed time series follows physical laws. Typically, \mathcal{D} is a discretisation of the explicit dynamics, formulated as a partial differential equation on the $N_t \times N_x \times N_y \times N_z$ grid, and the norm $\|\cdot\|$ can be either a squared L^2 , L^1 , TV , or Mahalanobis distance.

In this procedure, the physical model can be highly complex (in order to have satisfying resolution) and the major hurdle is then to express the adjoint operator of this model in order to compute the desired minimiser. This minimization problem is the one behind the 4DVar methods (Bocquet & Farchi, 2014). While the 3DVar strategy assimilates observations at a single time point without considering their temporal evolution, the 4DVar extends this approach by incorporating observations over a time window to better capture system dynamics, at the cost of increased computational complexity. Kalman filtering or extended version for non-linear systems such as Extended Kalman Filter (EKF) or Ensemble Kalman Filter (EnKF), on the other hand, adopt a probabilistic and sequential approach, updating the state estimate at each time step while dynamically propagating uncertainties, but remains computationally expensive, especially for nonlinear or large-scale systems.

Several attempts to include machine learning in these approach have already been explored (e.g., 4DVarNet) (Arcucci et al., 2021; Fablet et al., 2021; Beauchamp et al., 2023). Those methods combined standard assimilation techniques (cf. minimization of (1)) with neural network architecture either to build end-to-end approaches or a network improving the modeling of the map \mathcal{D} . More precisely, the network predicts $\mathbf{u}_{t+\Delta t}$ given \mathbf{u}_t and the regularisation term involves $\mathcal{D}(\mathbf{u}) = \mathbf{u}_{t+\Delta t} - f_\theta(\mathbf{u}_t)$, encouraging the reconstructed field \mathbf{u} to adhere to the learned dynamics modeled by the neural network denoted f_θ , with θ the network parameters. They show very promising results already comparable to the best classical approaches. For instance (Beauchamp et al., 2023) has reported a “*relative improvement with respect to the operational optimal interpolation between 30% and 60% in terms of reconstruction error*”. However, they are often implemented on surface reconstruction problems

and do not deal with the interior of the ocean due to a lack of data. Moreover, these methods are tied to a fixed grid, and as resolution increases, the cost of training the network can grow significantly.

2.2 PINNs

A second class of approaches that combine deep learning and physics models rely on the Physics-Informed Neural Network (PINN) framework and will be at the core of this contribution. The standard formulation of PINNs can be expressed as (1), with a key distinction: the field u is modeled by a neural network (i.e., $u = f_\theta(t, x)$) that uses spatio-temporal coordinates as inputs to predict the field values. In this work, following previous application to fluid mechanics problems (Raissi et al., 2019), we propose revisiting ocean data assimilation procedure using PINNs, which offer the key advantage of bypassing grid-based formulations that become computationally intensive when recovering 3d+t field such as subsurface fields.

We denote u_θ as a shallow neural network parameterized by θ , a function of (t, x) , whose output is the desired field for a specific spatio-temporal location. The PINN formulation reduces to finding the optimal network u_θ with parameters θ that minimize the following loss:

$$\mathcal{L}_{\text{PINN}}(\theta) = \frac{1}{n} \sum_{(t,x) \in \mathcal{I}} (u_\theta(t, x) - d(t, x))^2 + \lambda \|\mathcal{D}(u_\theta, \partial_t u_\theta, \nabla u_\theta, \dots)\|^2. \quad (2)$$

where \mathcal{I} denotes either a set of n points where measurements d are available (for data assimilation problems), a set of n points that sample initial and boundary conditions (to solve a well-posed Cauchy problem), or a combination of both. Initially, the formalism of PINNs has been developed to approach solutions to a well posed Cauchy problem with a chosen initial condition, boundary conditions and a chosen dynamics.

The loss function thus consists of a data term and a regularization term measuring deviation from the dynamical prior. It serves as an objective function that encourages the minimiser to both closely solve the prior PDE $\mathcal{D}(u, \partial_t u, \nabla u, \dots) = 0$ and ensure fidelity to the observations d . The norm $\|\mathcal{D}\|$ represents an L^2 norm over the spatio-temporal domain of interest, which must be approximated (e.g., using a Monte Carlo method). This involves evaluating the residual at a discrete set of collocation points that do not necessarily coincide with the data points.

The computation of the loss function assumes that the network u_θ can be differentiated with respect to its input coordinates to compute $\partial_t u_\theta$, $\partial_x u_\theta$, $\partial_y u_\theta$, and any higher-order derivatives required by the prior PDE. In practice, this step is straightforward due to automatic differentiation, which allows handling a wide range of differentiable functions u_θ . This is a major advantage of PINNs formulation. This approach is considered mesh-free because the field u is not discretized on a grid, unlike standard assimilation techniques.

In its original formulation, PINNs were implemented using a multilayer perceptron with a tanh activation function for u_θ , alongside a Latin Hypercube Sampling strategy to select collocation points where the PDE residual is computed (Raissi et al., 2019). Since then, significant efforts have focused on optimizing the choice of collocation points (Khoa Nguyen et al., 2022), exploring alternative network architectures (Wang et al., 2024), and testing different activation functions (Sitzmann et al., 2020), among other strategies (Karniadakis et al., 2021). The algorithmic strategy itself is rarely studied, as it generally relies on a single neural network fully trained using standard optimization tools. In this study, the specific layered structure of the underlying ocean dynamics will lead us to focus on both the choice of the architecture and the algorithmic strategy.

2.3 Focus on the implicit neural representation SIREN

In this study, we focus on the SIREN model, a fully connected network that uniquely employs sine activations after each layer, along with a specifically tailored network initialization (Sitzmann et al., 2020). More precisely, it has satisfying ability to learn simultaneously a function through its outputs and its gradients, thus our choice to use it in our study. This network architecture has proven useful in reconstructing various natural signals, including flow reconstruction with PINNs in the context of Rayleigh-Benard convection (Mommert et al., 2024). SIREN networks have also been used in ocean context, albeit without physical constraints, to represent surface current as a neural field (J. E. Johnson et al., 2022).

In this study, we will consider a SIREN network to describe $2d + t$ scalar fields :

$$\Psi_{\theta}(t, x, y) = W_M \cdot \sin(\dots W_2 \cdot \sin(W_1 \cdot \sin(K_x x + K_y y - \Omega_t t + \varphi) + b_1) + b_2) \dots + b_M \quad (3)$$

where sine functions are taken coordinate by coordinate. Network parameters are

$$\theta = \{K_x, K_y, \Omega_t, \varphi, W_1, \dots, W_M, b_1, \dots, b_M\},$$

where $K_x, K_y, \Omega_t \in \mathbb{R}^{w \times 1}$, $\varphi, b_m \in \mathbb{R}^w$, $W_m \in \mathbb{R}^{w \times w}$, $W_M \in \mathbb{R}^{1 \times w}$ and $b_M \in \mathbb{R}$.

This implicit neural representation takes field coordinates as inputs and outputs a scalar estimate of the field. The notion of resolution then shifts from a spatial resolution on a discretised domain to an implicit resolution related to the size of θ . Empirically, this implicit resolution corresponds to the spectral resolution. The smallest spatial and temporal scales that the SIREN can generate are limited by the highest values of K_x, K_y and Ω_t . Therefore, these values must be carefully initialized to ensure the network can capture the small physical scales in the signal.

SIREN is a particularly well-suited network for our task, as all activations are sine functions. Indeed, as a result, $\partial_t \mathbf{u}_{\theta}$ can also be expressed as a SIREN model with shifted weights, since the derivative of a sine function is another sine function with a shifted phase. This property extends to spatial derivatives and higher-order derivatives, such as the Laplacian operator Δ . The stability of SIREN models under differentiation heuristically explains, according to Sitzmann et al. (2020), why such a network model can impressively learn a function and its derivatives simultaneously. This characteristic makes it an ideal candidate for our purpose, which is to incorporate physical knowledge in the form of partial differential equations into the learning strategy. This network architecture was initially introduced to address image-related problems, but the authors also experimented it as a PINN to solve a simple linear wave-propagation equation. In the present contribution, we aim to fully exploit its potential for a more complex task.

3 StrAss-PINN : New Physics-Assisted Neural network for Data Assimilation in Stratified fluid

The proposed **StrAss**-PINN method builds on PINNs by adding a multilayer structure to both the training loss and the training process. In this section, we present the method through a concrete reconstruction problem for wind-driven, multilayer quasi-geostrophic dynamics, using ground truth from a simulation of a classic double-gyre setup. This setup models key features of midlatitude oceans, such as the Gulf Stream and the Kuroshio. Pseudo-observations will be extracted from this quasi-geostrophic ground truth, and the reconstruction will be compared to the full field of the simulation. For clarity, the method is presented here for a three-layer quasi-geostrophic model, though it can be extended to more layers. Details of the general multilayer formulation are provided in the Appendix Appendix A. Note to the reader: There are two notions of “layers”—oceanic layers and neural layers. We will clarify the context to avoid confusion whenever necessary.

3.1 Dynamical model: three-layer quasi-geostrophic dynamic

Layered structure of ocean models. Due to stable vertical density stratification and the small vertical-to-horizontal aspect ratio, ocean models are often represented as layers stacked on top of one another. In these models, stratification is defined by the density and horizontally averaged thickness of each layer. Many advanced ocean models use multilayer shallow water equations to capture large-scale stratification variations at the basin scale. By taking advantage of the large rotation limit relevant to midlatitude flows, one can then derive a simpler set of equations—the quasi-geostrophic model (Vallis, 2017). We focus here on a three layer quasi-geostrophic model driven by wind. The motivation is twofold: first, the quasi-geostrophic model filters out fast motions while capturing similar flow structures to the shallow water model, and second, three layers are sufficient to describe many important features of mid latitude mesoscale ocean current. The principal features being the intensification of western and surface currents, the propagation of Rossby waves, the formation of sharp eastward jets, and mesoscale vortex rings — hallmarks of oceanic turbulence. This model provides therefore a minimal framework for understanding midlatitude ocean currents like the Gulf Stream or Kuroshio (Vallis, 2017).

Flow model and parameters. We consider three layers of homogeneous density (ρ_1, ρ_2, ρ_3) stacked vertically, as shown in Fig. 2(a). In each layer, the flow is 2D, non-divergent, and can be described by stream functions (ψ_1, ψ_2, ψ_3), which fully characterize the dynamics as scalar functions of (t, x, y) . The flow takes place in a close basin with free slip boundary conditions. The system is forced by zonal wind stress curl $-\partial_y \tau_x(y)$, which drives the upper layer, and dissipates through the Ekman layer in the deeper layer, or via horizontal viscous dissipation in each layer. To capture key features of midlatitude ocean dynamics, we need to incorporate latitudinal variations in the Coriolis parameter using the β -plane approximation, which assumes linear variations of planetary vorticity with latitude. The resulting system of equations is expressed as the following set of partial differential equations:

$$\begin{aligned} \frac{d}{dt} \Big|_1 \underbrace{\left[\Delta\psi_1 - f_0^2 \frac{\psi_1 - \psi_2}{H_1 g'_1} + \beta y \right]}_{=q_1} &= -\frac{1}{H_1} \partial_y \tau_x + \nu \Delta q_1 \\ \frac{d}{dt} \Big|_2 \underbrace{\left[\Delta\psi_2 - f_0^2 \frac{\psi_2 - \psi_1}{H_2 g'_1} - f_0^2 \frac{\psi_2 - \psi_3}{H_2 g'_2} + \beta y \right]}_{=q_2} &= \nu \Delta q_2 \\ \frac{d}{dt} \Big|_3 \underbrace{\left[\Delta\psi_3 - f_0^2 \frac{\psi_3 - \psi_2}{H_3 g'_2} + \beta y \right]}_{=q_3} &= -r_E \Delta\psi_3 + \nu \Delta q_3 \end{aligned} \quad (4)$$

with $\frac{d}{dt} \Big|_\ell \equiv \partial_t + (\partial_x \psi_\ell) \partial_y - (\partial_y \psi_\ell) \partial_x$ representing the Lagrangian derivative, $g'_\ell = g \cdot (\rho_{\ell+1} - \rho_\ell) / \rho_\ell$ is the reduced gravity between the ℓ -th and $(\ell + 1)$ -th layers, and H_ℓ denotes the height of the ℓ -th layer. The parameter $r_E = f_0 h_E / 2H_3$ is the bottom friction coefficient, with f_0 the Coriolis parameter and h_E the Ekman layer depth. The double-gyre framework amounts to choosing $\tau_x = \tau_0 \cos(2\pi y/L)$, with L as the domain size and τ_0 the maximum wind stress amplitude. Additionally, we made the classical rigid assumption, which simplifies to assuming that $gH_\ell / f_0^2 \rightarrow +\infty$. Typical flow fields obtained with this model are shown in Fig. 2(b) for parameters presented in Tab. 1.

3.2 Posing the reconstruction problem with pseudo-observations

Our idealized quasi-geostrophic framework aims to address a typical ocean assimilation problem, where abundant surface data—usually from satellites like SWOT—are available, alongside sparser subsurface data—from ARGO floats. In real observations, ARGO floats typically provide measurements at a depth of 1 km for 9 days, then descend much deeper—usually to 2,000 meters, but up to 6,000 meters for deep-ARGO floats—before returning to the surface to transmit data and then resuming their descent. In our stratified

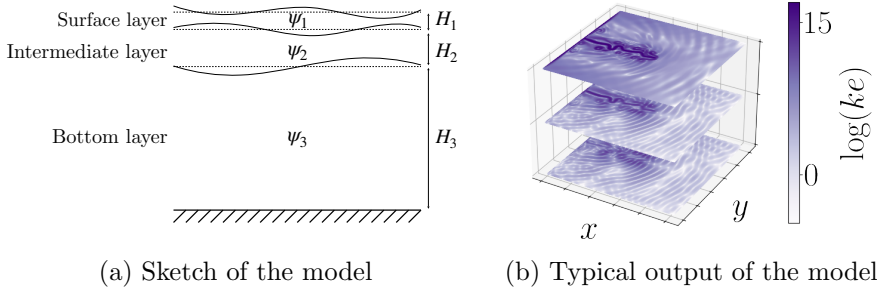


Figure 2: (a) Illustration of the three-layer framework with 2d flows in each layer encoded in stream functions ψ_i . (b) Kinetic energy fields in a three layers quasi-geostrophic model of the ocean. Three important features appear in the generated stream functions. First, as expected with the choice of wind forcing, two gyres are formed at the surface and induce a jet stream in the center of the domain. Second, we notice Rossby waves propagating in each layer. Third, small eddies go up the jet stream.

Coefficient	Value	Coefficient	Value
H_1	350 m	β	$1.7e - 11 \text{ m}^{-1} \cdot \text{s}^{-1}$
H_2	750 m	f_0	$9.4e - 5 \text{ s}^{-1}$
H_3	2900 m	τ_0	$1.3e - 5 \text{ m}^2 \cdot \text{s}^{-2}$
g'_1	$0.025 \text{ m} \cdot \text{s}^{-2}$	ν	$40 \text{ m}^2 \cdot \text{s}^{-1}$
g'_2	$0.0125 \text{ m} \cdot \text{s}^{-2}$	h_E	2 m
L	4000 km		

Table 1: Coefficients used in the implementation we study here.

framework, this process is represented by satellite data such as SWOT for the first layer, sparse random measurements for the second layer and even sparser observations for the third layer.

Concretely, following the notation in (2), we define a set of observation \mathcal{I}_ℓ for each layer $\ell = \{1, 2, 3\}$, incorporating SWOT-like measurements of ψ_1 , daily Argo-like measurements of ψ_2 , and Argo-like measurements of ψ_3 every 10 days, as shown in Fig. 3. The complete set of observations is denoted as $\mathcal{I} = \mathcal{I}_1 \cup \mathcal{I}_2 \cup \mathcal{I}_3$. More details about this set will be provided in subsection 4.1.

3.3 StrAss-PINN training network and loss

To train the network using partially observed data and evaluate it outside the observed domain, we design a multilayer algorithm, using the fact that the ocean model is represented by vertically stacked layers, each with homogeneous density but differing from one layer to the next in a stably stratified structure.

In the context of the three-layer quasi-geostrophic model, we consider three differential operators $\mathcal{D}_1, \mathcal{D}_2, \mathcal{D}_3$ allowing us to rewrite quasi-geostrophic dynamics (4) as:

$$\begin{cases} \mathcal{D}_1(\psi_1, \nabla \psi_2) = 0 \\ \mathcal{D}_2(\psi_2, \nabla \psi_1, \nabla \psi_3) = 0 \\ \mathcal{D}_3(\psi_3, \nabla \psi_2) = 0 \end{cases} \quad (5)$$

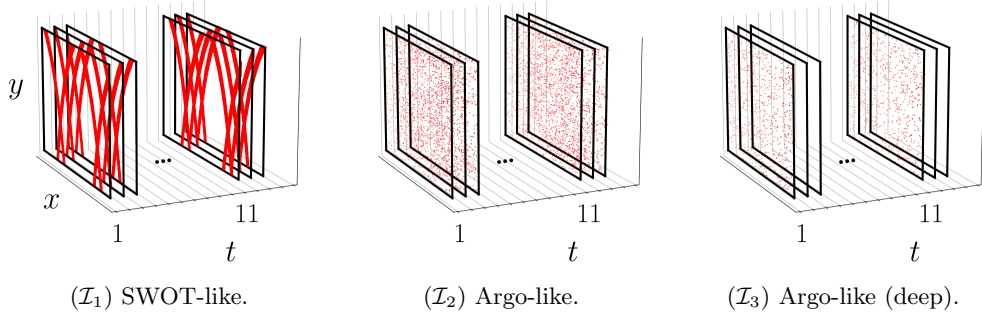


Figure 3: In our set-up, observations are only provided by pseudo-measurement devices at locations stored in \mathcal{I}_1 , \mathcal{I}_2 , and \mathcal{I}_3 . These three sets are illustrated here. Every simulation day, we have access to SWOT-like measurements of ψ_1 and Argo-like measurements of ψ_2 and every 10 simulation day we have Argo-like measurements of ψ_3 .

with $\nabla = (\partial_x, \partial_y)$. We note that each layer interacts only with the layers directly in contact with it, as illustrated in Fig. 2(a). For example, the second layer interacts nonlinearly with both the first and third layers. More generally, the operator \mathcal{D}_ℓ in layer ℓ involves only the streamfunction ψ_ℓ of the current layer and the spatial derivatives of $\psi_{\ell-1}$ and $\psi_{\ell+1}$, i.e., the velocity fields in the neighboring layers.

StrAss-PINN training network. This peculiar vertical structure of the flow model organized in layers encourages us to use separated networks to predict the stream functions and let them interact during their learning, instead of relying on a single network to generate direct estimates of (ψ_1, ψ_2, ψ_3) . In what follows, we will reconstruct the three fields of stream functions with three separate networks. We will use the following property: ψ_ℓ knows about $\nabla\psi_{\ell+1}$ and $\nabla\psi_{\ell-1}$ but not directly $\psi_{\ell+1}$ or $\psi_{\ell-1}$. Consequently, for each stratification layer ℓ , we design a network Ψ_{θ_ℓ} taking (t, x, y) as input allowing to estimate ψ_ℓ , with network parameters θ_ℓ . Each network will take the form of a SIREN as described in (3).

StrAss-PINN training loss. The proposed minimization problem aiming to estimate the parameters $(\theta_1, \theta_2, \theta_3)$ is formulated as the minimisation of the loss function $\mathcal{L}_{\text{StrAss-PINN}}$:

$$\mathcal{L}_{\text{StrAss-PINN}}(\theta_1, \theta_2, \theta_3) = \sum_{\ell=1}^3 \frac{1}{|\mathcal{I}_\ell|} \sum_{i \in \mathcal{I}_\ell} |\Psi_{\theta_\ell}(t_i, x_i, y_i, z_i) - d_i|^2 + \|\mathcal{D}_1(\Psi_{\theta_1}, \nabla\Psi_{\theta_2})\| + \|\mathcal{D}_2(\Psi_{\theta_2}, \nabla\Psi_{\theta_1}, \nabla\Psi_{\theta_3})\| + \|\mathcal{D}_3(\Psi_{\theta_3}, \nabla\Psi_{\theta_2})\|. \quad (6)$$

The quantity of interest are the estimated fields $\widehat{\psi}_\ell := \Psi_{\widehat{\theta}_\ell}$ with

$$(\widehat{\theta}_1, \widehat{\theta}_2, \widehat{\theta}_3) = \underset{(\theta_1, \theta_2, \theta_3)}{\operatorname{argmin}} \mathcal{L}_{\text{StrAss-PINN}}(\theta_1, \theta_2, \theta_3).$$

StrAss-PINN algorithmic strategy. In order to look for such a minimiser, we introduce a strategy guided by the stratified structure of the quasi-geostrophic model and the natural hierarchy between stratification layers. We propose to learn each oceanic layer successively starting from the surface down to the deep layer as sketched in Fig. 4 and explained as follows. Such a strategy is a block-minimization procedure that consists in solving, for each

iteration k ,

$$\begin{aligned}\theta_1^{[k+1]} &= \operatorname{argmin}_{\theta_1} \underbrace{\sum_{i \in \mathcal{I}_1} |\Psi_{\theta_1}(t_i, x_i, y_i) - d_i|^2 + \left\| \mathcal{D}_1 \left(\Psi_{\theta_1}, \nabla \Psi_{\theta_2^{[k]}} \right) \right\|}_{\mathcal{L}_{\text{StrAss-PINN}}^{(1)}(\theta_1, \theta_2^{[k]})} \\ \theta_2^{[k+1]} &= \operatorname{argmin}_{\theta_2} \underbrace{\sum_{i \in \mathcal{I}_2} |\Psi_{\theta_2}(t_i, x_i, y_i) - d_i|^2 + \left\| \mathcal{D}_2 \left(\Psi_{\theta_2}, \nabla \Psi_{\theta_1^{[k+1]}}, \nabla \Psi_{\theta_3^{[k]}} \right) \right\|}_{\mathcal{L}_{\text{StrAss-PINN}}^{(2)}(\theta_1^{[k+1]}, \theta_2, \theta_3^{[k]})} \\ \theta_3^{[k+1]} &= \operatorname{argmin}_{\theta_3} \underbrace{\sum_{i \in \mathcal{I}_3} |\Psi_{\theta_3}(t_i, x_i, y_i) - d_i|^2 + \left\| \mathcal{D}_3 \left(\Psi_{\theta_3}, \nabla \Psi_{\theta_2^{[k+1]}} \right) \right\|}_{\mathcal{L}_{\text{StrAss-PINN}}^{(3)}(\theta_2^{[k+1]}, \theta_3)}\end{aligned}$$

Once the training of Ψ_{θ_1} has converged, we can compute an estimation of $\nabla \Psi_{\theta_1}$ that we freeze (meaning we stop learning θ_1) in order to define the approximate differential operator $\mathcal{D}_2(\cdot, \nabla \Psi_{\theta_1}, \cdot)$ and start learning the parameters of Ψ_{θ_2} using the loss $\mathcal{L}_{\text{StrAss-PINN}}^{(2)}$. Finally, we construct \mathcal{D}_3 similarly using a frozen estimate of $\nabla \Psi_2$ to learn the parameters of Ψ_{θ_3} using the loss $\mathcal{L}_{\text{StrAss-PINN}}^{(3)}$. The circulation of information is sketched in the diagram Fig. 4, and the algorithm is summed up in Alg. 1.

StrAss-PINN initialization. The algorithm procedure is initialized with $\Psi_{\theta_2^{[0]}} = \Psi_{\theta_3^{[0]}} = 0$. The motivation behind the choice $\Psi_{\theta_2^{[0]}} = 0$ is that the flow is much stronger at the surface than in the interior of the domain, i.e. $\nabla \psi_1 \gg \nabla \psi_2$. Therefore, a fair approximation for \mathcal{D}_1 is to consider $\nabla \psi_2 = 0$ everywhere. Similarly, the flow in the intermediate layer is much stronger than in the abyss, hence the choice $\Psi_{\theta_3^{[0]}} = 0$. This strategy uses prior knowledge of ocean dynamics, which are typically surface-intensified. In some specific cases, such as above seamounts, the dynamics may instead be bottom-intensified. In that context, the algorithm's convergence may not be optimal. We will explore more efficient strategies to account for these situations in future work.

Algorithm 1 StrAss-PINN

Require: Observations points: $(\mathcal{I}_1, \mathcal{I}_2, \mathcal{I}_3)$ and $\{(t_i, x_i, y_i, d_i)\}_{i \in \mathcal{I}_\ell}$ for $\ell = 1, 2, 3$.

Collocation points: $\{(T_j, X_j, Y_j)\}_{j \in \mathcal{J}}$.

while $\mathcal{L}_{\text{StrAss-PINN}} \geq \varepsilon$ **do**

for $k=1$ to K **do**

 Get batches from \mathcal{I} and define collocation points

$$\theta_1^{[k+1]} = \operatorname{argmin}_{\theta_1} \mathcal{L}_{\text{StrAss-PINN}}^{(1)}(\theta_1, \theta_2^{[k]})$$

$$\theta_2^{[k+1]} = \operatorname{argmin}_{\theta_2} \mathcal{L}_{\text{StrAss-PINN}}^{(2)}(\theta_1^{[k+1]}, \theta_2, \theta_3^{[k]})$$

$$\theta_3^{[k+1]} = \operatorname{argmin}_{\theta_3} \mathcal{L}_{\text{StrAss-PINN}}^{(3)}(\theta_2^{[k+1]}, \theta_3)$$

end for

end while

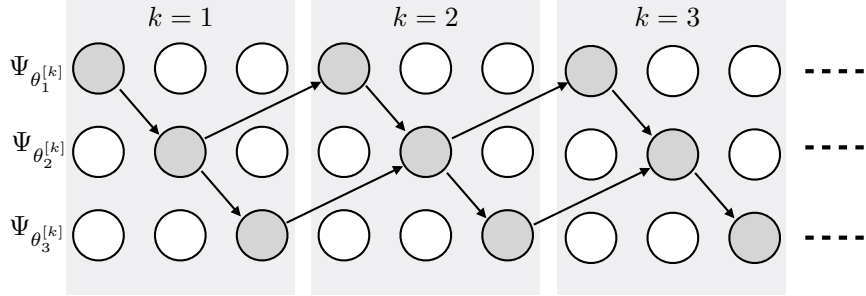


Figure 4: Circulation of the information in the proposed multilayer optimisation process. This illustration is provided for the three first iterations for the 3-layer quasi-geostrophic dynamics but can easily be generated to N layers introducing N networks alternatively learning.

4 Numerical experiments

4.1 Data

Ground truth simulation – The ground truth (ψ_1, ψ_2, ψ_3) are obtained from the three layers quasi-geostrophic model of the ocean introduced section 3.1. The values implemented in the studied simulation are summarized in Tab. 1. The lengthscales of the system are: the size of the domain $L = 4000$ km and the two Rossby deformation radii are $L_1 \sim 39$ km, $L_2 \sim 22$ km. The corresponding timescales are of order $T = 1/(\beta L_i) \sim 22$ days.

Typical flow fields obtained with this model are shown in Fig. 2. In the upper layer, a western-intensified front is visible at the interface between two large-scale gyres, corresponding to a coherent eastward jet similar to the Gulf Stream or Kuroshio. Coherent eddies can also be seen propagating westward, corresponding to mesoscale oceanic rings. Additionally, Rossby waves propagate across the entire domain, with their phase moving westward. In the interior layers (Fig. 2(b)), the front, eddies, and waves are still present, supporting our hypothesis that surface data can be used to help assimilate ocean interior information. To summarize, this ground truth simulation features simple yet interesting flow structures, both horizontally and vertically, making it an ideal framework for validating our reconstruction method.

Pseudo-observations \mathcal{I} – From these simulated data, we constructed pseudo-observations, motivated by the framework presented in section 3.2, to combine SWOT-like data and ARGO-like data. Recall that the pseudo-observation locations are organized into three sets, \mathcal{I}_ℓ , each associated with a layer ℓ , and we make the simplifying assumption that a measurement in layer ℓ corresponds to an observation of ψ_ℓ .

The set \mathcal{I}_1 in the surface layer is obtained by constructing a mask that replicates the trace of a virtual SWOT-like satellite observation of sea surface height (ψ_1), following Le Guillou et al. (2021). To do this, we virtually placed our $4000 \text{ km} \times 4000 \text{ km}$ ocean basin over the North Atlantic Ocean, at latitudes consistent with the Coriolis parameter $f_0 + \beta_0 y$. We then used the coordinates of the actual satellite’s SWOT trajectory and its two swaths, as if it passed over that domain. \mathcal{I}_1 is the set of (t, x, y) coordinates for which the point (x, y) belongs to one of the swaths of SWOT at time t . Over a period of 100 days, this results in a total of 392,470 observation points, *i.e.*, approximately 1.5% of the domain being observed each day.

The set \mathcal{I}_2 in the intermediate layer corresponds to the locations of 800 independent ARGO-like buoys measuring ψ_2 . Each day, the buoys are randomly distributed across the

513 × 513 domain grid. This is a realistic, though somewhat exaggerated, amount of ARGO data for the size of our domain (Argo, 2024).

The set \mathcal{I}_3 in the deeper layer is also obtained by randomly selecting 800 buoys in the 513 × 513 grid points, but the daily averages of the streamfunction are measured only every ten days, consistent with the behavior of ARGO floats that dive every 10 days.

To facilitate this preliminary analysis, we assume that measurements always provide direct information about the streamfunction in the observed layer. While this assumption is reasonable for the low-frequency component of sea surface height measurements from altimetry, it is an oversimplification for ARGO measurements, which provide information on thermodynamic variables rather than direct streamfunction data. However, under the assumption of geostrophic and hydrostatic balance, these measurements can be related to vertical variations in the streamfunction, rather than the streamfunction itself. Future work will focus on developing a more realistic representation of these measurements.

4.2 Algorithm

Neural network architecture. We deploy three SIREN neural networks, one for each layer. In our experiments we explore the impact of Ω_t, K_x, K_y , controlling the weights of SIREN’s first layer as they are the only parameters of the network that can directly be physically interpreted. In their paper, Sitzmann et al. (2020) set a maximal value ω_0 for this first layer and initialise the weight uniformly between $-\omega_0$ and ω_0 . Conducting numerical experiments, we noticed in our case that these values do not change significantly during the learning. We thus decided to remove that randomness and set the values of the first layer in the following way. First, we chose a maximal value for the pulsation ω_{max} and one for the wave numbers k_{max} . Then we fill Ω_t with N uniformly spread numbers between $-\omega_{max}$ and ω_{max} , K_x with N uniformly spread numbers between $-k_{max}$ and k_{max} and finally K_y with N uniformly spread numbers between 0 and k_{max} . This way, the first layer covers a wide variety of potential waves propagating in our domain of the form $\sin(k_x x + k_y y - \omega_t t)$ with $k_x \in K_x, k_y \in K_y$ and $\omega_t \in \Omega_t$. This choice leads to N^3 waves. Choosing $N = 5$ is what set the width of our network to equal 125. Note that adding negative values for k_x does not express more waves as the sine function is odd.

Collocation points \mathcal{J} . Other important parameters to adjust that can affect the training of the network are the number and the location of the collocation points. The higher it is, the better the estimation of $\|\mathcal{D}(\cdot)\|_{L^2(\Omega)}$. However, the number of collocation point to consider is limited by the memory capacity of the machine used. We opted for `N_col` = 13 × `batch_size_col` = 266240. Compared to literature, this is relatively few as we only have `N_col` ≈ 10 × `N_obs`. It is usually recommended to have two or more orders of magnitude difference between `N_obs` and `N_col` but we had satisfying results with this set-up. Adding more collocation points would significantly increase the memory requirements of the method and probably call for multi-GPU training, which we did not explore.

Minimization strategy for $\mathcal{L}_{\text{StrAss-PINN}}^{(\ell)}$. We look for the minimiser of the loss function using the gradient-based optimizer ADAM with learning rate of 1e-4 and batches of size 1/13 of the total available data. In accordance with other PINNs formulation, the input and output are normalized. This is detailed in appendix Appendix C. All experiments were executed on a machine with an Intel Xeon Platinum 9242 CPU and an AD104GL [L4] GPU with 16 GB of RAM.

Regularization parameter. The main parameter to tune is the regularisation parameter λ , the ratio of the data fidelity loss term to the physic-informed loss term \mathcal{L}_{dyn} . It balances these two parts of the objective function and controls how much the network trusts the observations during its learning and how much the reconstruction is a physical field. A high value for λ will thus lead to a very smooth reconstruction. We chose $\lambda = 0.0001$ following the results shown in section 4.3.

The values of the hyper-parameters used in the following numerical experiments are summarized in Tab. 2.

Parameter	Value	Parameter	Value
N_obs_surf	392470	N_obs_int	80000
N_obs_bot	8000	N_col	266240
bs_obs	30190	bs_col	20480
k_{max}	10	ω_{max}	1.5
λ	1e-4	learning rate	1e-4

Table 2: Summary of the choices of hyper-parameters values in the network.

4.3 Results

Recovery illustration. The results presented in Fig. 5 are obtained after one step of the alternate scheme 1 on pseudo-observations for a period of 100 days. We were able to reconstruct not only the surface field but also the ones in the interior of the ocean, leveraging physics knowledge to help the information propagate downward. Physically, it is very interesting to see that the reconstructed stream functions include the physical features resolved by the explicit model. Namely, the jet and the vortices detaching from it are well resolved even though they are poorly observed. It also resolved the large scale waves visible mainly in the right part of the domain for the first layer and everywhere for the other two. It is notable to remark that we were able to represent a field with original resolution $N = 1,638,400$ in a simulation at a resolution of $100 \times 128 \times 128$ with only $3 \times w + w + 2 \times (w \times w + w) + w + 1 = 32126$ parameters in **StrAss-PINN**.

Impact of the regularisation parameter λ . This is an important parameter to tune as it can guide the learning towards a more significant reconstruction even with fewer observations. However, it can yield a degraded reconstruction if wrongly set. The difference in the quality of reconstruction when no regularisation, *i.e.* $\lambda = 0$, the right amount of regularisation, $\lambda = 10^{-4}$ or to much regularisation is applied is shown in Fig. 6 at a specific time. Visually, displaying the reconstruction into a small movie shows that structure in the reconstruction without regularisation are less smooth than those with regularisation (*i.e.*, jumps in wave phase). Additionally, in the left column, with increased regularization (*i.e.*, $\lambda = 1$), the field becomes smoother, especially for the first layer. The right panel of Fig. 6 shows the difference between the reconstructed fields on the left and the ground truth simulation, available everywhere in the domain, *i.e.* the reconstruction error. Qualitatively, one can see less structure in the error field with $\lambda = 10^{-4}$ than with $\lambda = 0$ or $\lambda = 1$. This shows the reconstruction captured more faithfully the physical features of the flow. Quantitatively, the mean square value of this difference is lower when some regularisation is used. The reconstruction scores evaluated on a 128×128 space grid and averaged over the 100 days of assimilation are shown in Tab. 3.

Impact of SIREN initialisation. As mentioned above, the initialisation of the layers of SIREN can impact the quality of the reconstructed fields. Exploring the space of hyper-parameters by hand, we found the set of values showed in Tab. 2 to work very well and the value of the reconstruction error to be stable around these values.

Impact of SIREN architecture. The number of layers and of neurons per layer were kept low in order to keep a model as transparent as possible for us to choose the just mentioned hyper-parameters by hand.

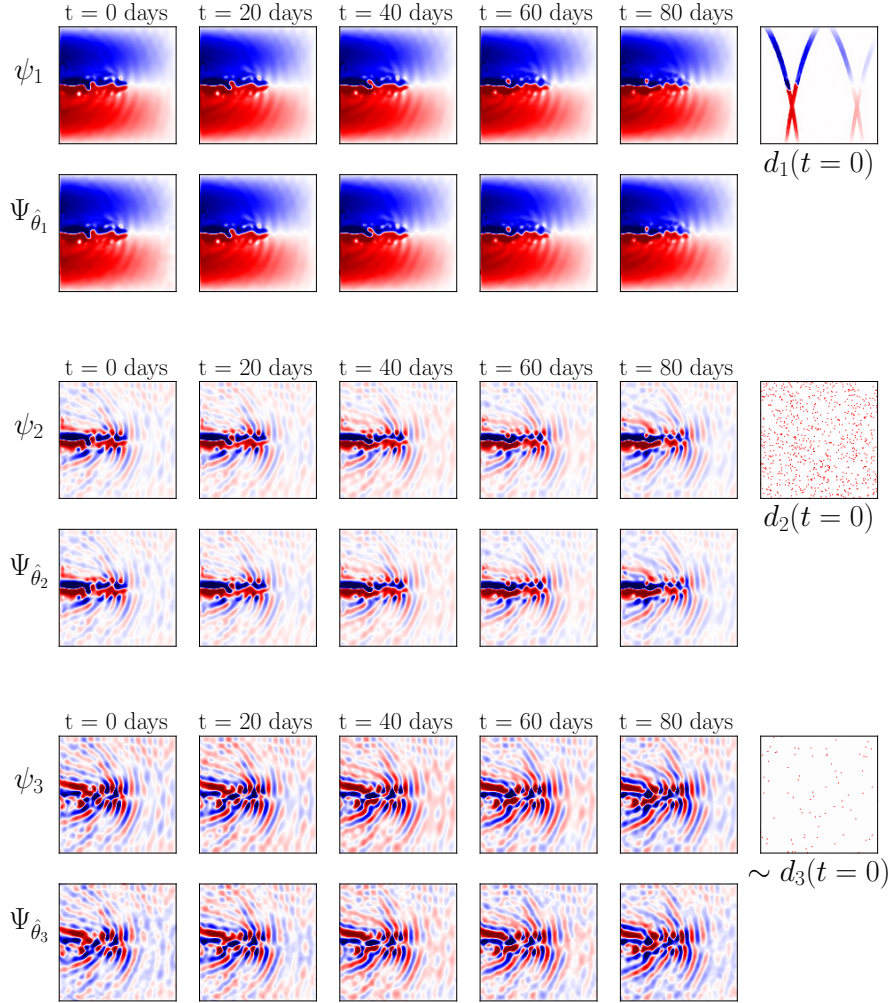


Figure 5: Reconstructed stream functions in each oceanic layer of the quasi-geostrophic model compared to the full simulated fields. A snapshot of the observation points is shown next to the reconstruction to have an idea of the available data. Note that for the bottom layer, these observations are only available every ten days. Physically, it is very interesting to see that the reconstructed stream functions include the physical features resolved by the explicit model. Namely, the jet and the vortices detaching from it are well resolved even though they are poorly observed. It also resolved the large scale waves visible mainly in the right part of the domain for the first layer and everywhere for the other two.

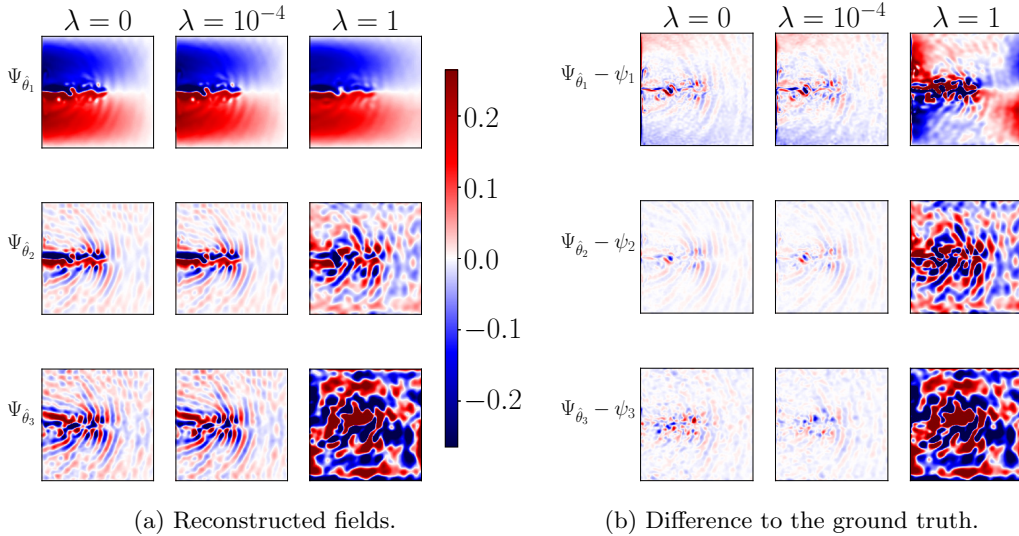


Figure 6: (a) reconstructed fields at a single time step and (b) the difference to the ground truth simulation for three reconstruction results: no regularisation (i.e. $\lambda = 0$), the right amount of regularisation (i.e. $\lambda = 10^{-4}$), or too much regularisation (i.e., $\lambda = 1$). Qualitatively, one can see from reconstruction error less structure with $\lambda = 10^{-4}$ than with $\lambda = 0$, showing that the reconstruction captured more faithfully the physical features of the flow.

λ	Surface MSE	Intermediate MSE	Abyss MSE
0	53.72	0.79	4.02
10^{-4}	36.98	0.94	2.17
1	279.99	264.03	1548.08

Table 3: Mean square error of the reconstruction to the ground truth simulation multiplied by a factor 10^4 for clarity. Error in the reconstruction of the deep field was nearly halved using the physics-informed loss as regularisation with the right balance to the data term.

Reconstruction using noisy data. In order to evaluate the stability of the method to noisy data, we add white Gaussian noise with standard deviation of 0.05 and re-run our experiments. We can clearly observe that **StrAss-PINN** successfully reconstructs the field and, as expected, the required regularization parameter needs to be set higher for larger standard deviations in the noise distribution. The illustration for the standard deviation set to 0.05 is provided in Appendix Appendix B.

5 Discussion and conclusions

We have shown that **StrAss-PINN** is a promising tool for ocean data assimilation by using an idealized three-layer quasi-geostrophic ocean model as the "ground truth" and realistic pseudo-observations resembling surface SWOT-like data and interior ARGO-like data. This minimal setup is relevant for assessing the feasibility of reconstructing deep ocean flows.

The first advantage of **StrAss-PINN** and PINNs in general is that they do not rely on a predefined grid mesh. While there is still an implicit resolution (determined by the

number of network parameters), **StrAss**-PINN can enhance the resolution of the initial field. For example, if there is a missing day of observations, the resolution can be increased in the model. A second advantage is that, for data assimilation problems like the one considered here, there is no need for knowledge of boundary or initial conditions in the loss function. The third advantage of encoding the ocean field in a network is the highly effective representation of the 3d field. This ability to compress information while maintaining well-behaved derivatives opens up potential for future work in ocean data assimilation.

Several challenges remain to be addressed in future research in order to reconstruct real ocean flows effectively with **StrAss**-PINN. First, we will need to determine the minimal amount of data needed for accurate flow reconstruction, exploring this question for each ocean layer independently. It will also be important to assess PINNs' performance in comparison to more traditional assimilation techniques, such as 4DVar. Second, there is significant potential to improve the efficiency of the PINN strategy used in this study. For example, the selection of collocation points used to estimate the physical constraints in the cost function can be optimized, as has been proposed in previous work (Nabian et al., 2021; Khoa Nguyen et al., 2022). Finally, the approach will need to be extended to multilayer shallow water models and eventually to more comprehensive ocean models, up to real-world data.

In summary, this paper demonstrates the potential of Physics-Informed Neural Networks for reconstructing three-dimensional ocean currents from abundant surface data and sparse interior measurements. The novelty of our method lies in its ability to reconstruct not only surface but also deep ocean currents in this context. By combining available data with the underlying dynamics of ocean circulation, PINNs offer a promising approach for inferring deep ocean dynamics. Our study serves as a proof of concept for applying PINNs to deep ocean flow reconstruction.

Appendix A Multilayer StrAss-PINN in the general setting

In the proposed model, we consider L differential operators $(\mathcal{D}_\ell)_{1,\dots,L}$ allowing us to rewrite quasi-geostrophic dynamics (4) as:

$$\begin{cases} \mathcal{D}_1(\psi_1, \nabla\psi_2) = 0 \\ \mathcal{D}_\ell(\psi_\ell, \nabla\psi_{\ell-1}, \nabla\psi_{\ell+1}) = 0 & \forall \ell = 2, \dots, L-1 \\ \mathcal{D}_L(\psi_L, \nabla\psi_{L-1}) = 0 \end{cases} \quad (\text{A1})$$

The optimisation problem we now have to face is then to find a set $(\theta_1, \dots, \theta_{L-1})$ of parameters that minimise the training loss function $\mathcal{L}_{\text{StrAss-PINN}}$:

$$\begin{aligned} \mathcal{L}_{\text{StrAss-PINN}}(\Psi_{\theta_1}, \dots, \Psi_{\theta_L}) &= \frac{1}{n} \sum_{i=1}^n |u_\theta(t_i, x_i, y_i, z_i) - d_i|^2 + \|\mathcal{D}_1(\Psi_{\theta_1}, \nabla\Psi_{\theta_2})\| \\ &+ \sum_{\ell=1}^{L-1} \|\mathcal{D}_\ell(\Psi_{\theta_\ell}, \nabla\Psi_{\theta_{\ell-1}}, \nabla\Psi_{\theta_{\ell+1}})\| + \|\mathcal{D}_L(\Psi_{\theta_L}, \nabla\Psi_{\theta_{L-1}})\| \end{aligned} \quad (\text{A2})$$

In order to look for such a minimiser, we introduce a strategy guided by the stratified structure of the quasi-geostrophic model and the natural hierarchy between stratification layers. We propose to learn each oceanic layer successively starting from the surface down as sketched in Fig. 4 and explained as follows. Such a strategy is a block-minimization procedure that consists in solving

$$\begin{aligned} &\min_{\theta_1} \sum_{i \in \mathcal{I}_1} |u_\theta(t_i, x_i, y_i, z_i) - d_i|^2 + \|\mathcal{D}_1(\Psi_{\theta_1}, \nabla\Psi_{\theta_2})\| \\ &\min_{\theta_2} \sum_{i \in \mathcal{I}_2} |u_\theta(t_i, x_i, y_i, z_i) - d_i|^2 + \|\mathcal{D}_2(\Psi_{\theta_2}, \nabla\Psi_{\theta_1}, \nabla\Psi_{\theta_3})\| \\ &\quad \vdots \\ &\min_{\theta_{L-1}} \sum_{i \in \mathcal{I}_{L-1}} |u_\theta(t_i, x_i, y_i, z_i) - d_i|^2 + \|\mathcal{D}_{L-1}(\Psi_{\theta_{L-1}}, \nabla\Psi_{\theta_{L-2}}, \nabla\Psi_{\theta_L})\| \\ &\min_{\theta_L} \sum_{i \in \mathcal{I}_L} |u_\theta(t_i, x_i, y_i, z_i) - d_i|^2 + \|\mathcal{D}_L(\Psi_{\theta_L}, \nabla\Psi_{\theta_{L-1}})\| \end{aligned}$$

Appendix B Noisy data

In order to test the stability of our method to noisy data, we artificially added to each pseudo-observation a Gaussian noise of standard deviation 0.05. The result is shown in Fig. B1. **StrAss-PINN** successfully reconstructs the fields significantly more accurately than the option without regularisation which overfits the noisy observations. As expected, the required regularization parameter needs to be set higher for larger standard deviations of the noise than with untouched data.

Appendix C Data normalisation

It is a widely spread information that neural networks tend to prefer normalised inputs and outputs. In order to fit with this idea, we transform the domain from $\Omega = [0, T] \times [0, L]^2$ to $\tilde{\Omega} = [-1, 1]^3$ and the outputs are normalised as well:

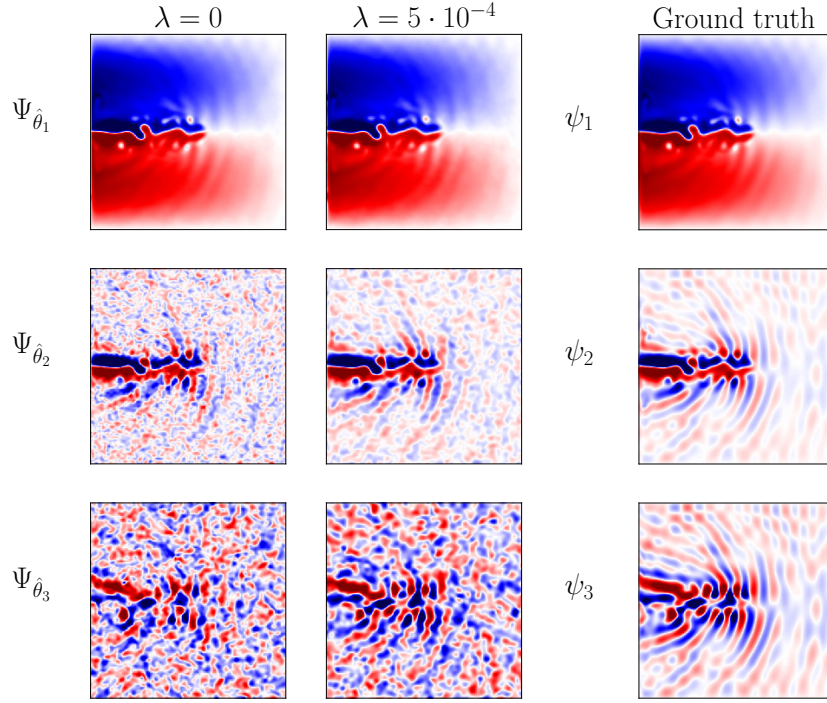


Figure B1: Reconstruction with noisy pseudo-observations.

$$\begin{aligned}
 \psi_1 &\leftarrow (\psi_1 - \mu)/\sigma \\
 \psi_2 &\leftarrow (\psi_2 - \mu)/\sigma \\
 \psi_3 &\leftarrow (\psi_3 - \mu)/\sigma
 \end{aligned} \tag{C1}$$

with μ and σ the mean and standard deviation of the observed data for the first layer.

Now we need to rewrite the transformed differential operators. The advection operators now read:

$$\left. \frac{d}{dt} \right|_i = r_t \partial_t + r_x^2 [-\partial_y (\sigma \Psi_i) \cdot \partial_x + \partial_x (\sigma \Psi_i) \cdot \partial_y] \tag{C2}$$

Let us write things explicitly for \mathcal{D}_1 . For given networks Ψ_1 and Ψ_2 encoding the stream functions in the two first layers, the corresponding encoded potential vorticity \tilde{Q}_1 is:

$$\tilde{Q}_1 = r_x^2 \Delta (\sigma \Psi_1) + \frac{\sigma \Psi_2 - \sigma \Psi_1}{L_1^2} + \beta \frac{\tilde{y}}{r_x} \tag{C3}$$

with $r_t = 2/T$ and $r_x = 2/L$. And the operator now reads:

$$\begin{aligned}
\mathcal{D}_1(\Psi_1, \nabla\tilde{\Psi}_2, \Delta\tilde{\Psi}_2) &= \frac{d}{dt}\Big|_1 \left(r_x^2 \Delta(\sigma\Psi_1) - \frac{\sigma\Psi_1}{L_1^2} \right) \\
&+ \frac{\sigma}{L_1^2} \frac{d}{dt}\Big|_1 \Psi_2 \\
&+ r_x \beta \partial_{\tilde{x}}(\sigma\Psi_1) \\
&- r_x \frac{\tau_0}{H_1} \pi \sin(\pi\tilde{y}) + \nu r_x^2 \Delta\tilde{Q}_1
\end{aligned} \tag{C4}$$

The same treatment was done to \mathcal{D}_2 and \mathcal{D}_3 .

Open Research Section

The codes implementing **StrAss**-PINN are published in the Zenodo repository

<https://zenodo.org/records/15075427>

and the idealized ocean simulation data sets (including pseudo-observations) are published in the Zenodo repository

<https://doi.org/10.5281/zenodo.15074965> .

Acknowledgments

BD warmly thanks Emmanuel Cosme for useful discussions on deep flow reconstruction in data assimilation. The authors also thank the CBPSMN platform at ENS-Lyon for providing efficient computing resources for all the necessary numerical experiments. The platform uses SIDUS (Quemener & Corvellec, 2013), which was developed by Emmanuel Quemener.

References

- Archambault, T., Filoche, A., Charantonis, A., Béréziat, D., & Thiria, S. (2024). Learning sea surface height interpolation from multi-variate simulated satellite observations. *Journal of Advances in Modeling Earth Systems*, 16(6), e2023MS004047.
- Arcucci, R., Zhu, J., Hu, S., & Guo, Y.-K. (2021). Deep data assimilation: Integrating deep learning with data assimilation. *Applied Sciences*, 11(3). doi: 10.3390/app11031114
- Argo. (2024). *Argo (oceanography)* — *Wikipedia, the free encyclopedia*. Retrieved from [https://en.wikipedia.org/wiki/Argo_\(oceanography\)](https://en.wikipedia.org/wiki/Argo_(oceanography)) ([Online; accessed 12-December-2024])
- Ballarotta, M., Ubelmann, C., Pujol, M.-I., Taburet, G., Fournier, F., Legeais, J.-F., ... others (2019). On the resolutions of ocean altimetry maps. *Ocean science*, 15(4), 1091–1109.
- Bang, C., Altaher, A. S., Zhuang, H., Altaher, A., Srinivasan, A., & Cherubin, L. (2024). Physics-informed neural networks to reconstruct surface velocity field from drifter data. *Authorea Preprints*.
- Barth, A., Alvera-Azcárate, A., Licer, M., & Beckers, J.-M. (2020). Dincae 1.0: A convolutional neural network with error estimates to reconstruct sea surface temperature satellite observations. *Geoscientific Model Development*, 13(3), 1609–1622.
- Beauchamp, M., Febvre, Q., Georgenthum, H., & Fablet, R. (2023). 4DVarNet-SSH: End-to-end learning of variational interpolation schemes for nadir and wide-swath satellite altimetry. *Geoscientific Model Development*, 16(8), 2119–2147.
- Blayo, É., Bocquet, M., Cosme, E., & Cugliandolo, L. F. (2014). *Advanced data assimilation for geosciences: Lecture notes of the les houches school of physics: Special issue, june 2012*. OUP Oxford.
- Bocquet, M., & Farchi, A. (2014). *Introduction to the principles and methods of data assimilation in the geosciences*. Retrieved from <https://ceraa.enpc.fr/HomePages/bocquet/teaching/assim-mb-en.pdf>
- Carrassi, A., Bocquet, M., Bertino, L., & Evensen, G. (2018). Data assimilation in the geosciences: An overview of methods, issues, and perspectives. *Wiley Interdisciplinary Reviews: Climate Change*, 9(5), e535.
- Clark Di Leoni, P., Agasthya, L., Buzzicotti, M., & Biferale, L. (2023). Reconstructing rayleigh-bénard flows out of temperature-only measurements using physics-informed neural networks. *The European Physical Journal E*, 46(3), 16.
- Fablet, R., Chapron, B., Drumetz, L., Mémin, E., Pannekoucke, O., & Rousseau, F. (2021, October). Learning variational data assimilation models and solvers. *Journal of Advances in Modeling Earth Systems*, 13(10).
- Fablet, R., Chapron, B., Le Sommer, J., & Sévellec, F. (2024). Inversion of sea surface currents from satellite-derived sst-ssh synergies with 4dvarnets. *Journal of Advances*

- in *Modeling Earth Systems*, 16(6), e2023MS003609.
- Fox-Kemper, B., Hewitt, H. T., Xiao, C., Aalgeirsdóttir, G., Drijfhout, S. S., Edwards, T. L., ... others (2021). Ocean, cryosphere, and sea level change. In *Climate change 2021: The physical science basis. contribution of working group I to the sixth assessment report of the intergovernmental panel on climate change* (pp. 1211–1361). Cambridge University Press.
- Fu, L.-L., Christensen, E. J., Yamarone Jr, C. A., Lefebvre, M., Menard, Y., Dorrer, M., & Escudier, P. (1994). *Topex/poseidon mission overview* (Vol. 99) (No. C12). Wiley Online Library.
- Fu et al, L.-L. (2024). The surface water and ocean topography mission: A breakthrough in radar remote sensing of the ocean and land surface water. *Geophys. Res. Lett.*, 51(4), e2023GL107652.
- Guinehut, S., Dhomps, A.-L., Larnicol, G., & Le Traon, P.-Y. (2012). High resolution 3-d temperature and salinity fields derived from in situ and satellite observations. *Ocean Science*, 8(5), 845–857.
- Johnson, G. C., & King, B. A. (2023). Zapiola gyre, velocities and mixing, new argo insights. *Journal of Geophysical Research: Oceans*, 128(6), e2023JC019893.
- Johnson, J. E., Lguensat, R., Fablet, R., Cosme, E., & Le Sommer, J. (2022). Neural fields for fast and scalable interpolation of geophysical ocean variables. *arXiv preprint arXiv:2211.10444*.
- Karniadakis, G. E., Kevrekidis, I. G., Lu, L., Perdikaris, P., Wang, S., & Yang, L. (2021). Physics-informed machine learning. *Nature Reviews Physics*, 3(6), 422–440.
- Khoa Nguyen, T. N., Dairay, T., Meunier, R., Millet, C., & Mougeot, M. (2022). Fixed-budget online adaptive learning for physics-informed neural networks. towards parameterized problem inference. *arXiv e-prints*, arXiv–2212.
- Le Guillou, F., Metref, S., Cosme, E., Ubelmann, C., Ballarotta, M., Le Sommer, J., & Verron, J. (2021). Mapping altimetry in the forthcoming SWOT era by back-and-forth nudging a one-layer quasigeostrophic model. *J. Atmos. Oceanic Technol.*, 38(4), 697–710.
- Lellouche, J.-M., Greiner, E., Bourdallé-Badie, R., Garric, G., Melet, A., Drévilion, M., ... others (2021). The copernicus global 1/12 oceanic and sea ice glorys12 reanalysis. *Frontiers in Earth Science*, 9, 698876.
- Lucor, D., Agrawal, A., & Sergent, A. (2022). Simple computational strategies for more effective physics-informed neural networks modeling of turbulent natural convection. *Journal of Computational Physics*, 456, 111022.
- Manucharyan, G. E., Siegelman, L., & Klein, P. (2021). A deep learning approach to spatiotemporal ssh interpolation and estimation of deep currents in geostrophic ocean turbulence. *Journal Of Advances In Modeling Earth Systems*, 13(1).
- Martin, S. A., Manucharyan, G. E., & Klein, P. (2023). Synthesizing sea surface temperature and satellite altimetry observations using deep learning improves the accuracy and resolution of gridded sea surface height anomalies. *Journal of Advances in Modeling Earth Systems*, 15(5), e2022MS003589.
- Millet, C., Khoa Nguyen, T. N., & Mougeot, M. (2023). Physics-informed learning for modeling infrasound propagation in extreme weather conditions. *The Journal of the Acoustical Society of America*, 154(4-supplement), A269–A269.
- Mommert, M., Barta, R., Bauer, C., Volk, M.-C., & Wagner, C. (2024). Periodically activated physics-informed neural networks for assimilation tasks for three-dimensional rayleigh-benard convection. *arXiv preprint arXiv:2403.02970*.
- Munk, W., Worcester, P., & Wunsch, C. (1995). *Ocean acoustic tomography*. Cambridge University Press.
- Nabian, M. A., Gladstone, R. J., & Meidani, H. (2021, April). Efficient training of physics-informed neural networks via importance sampling. *Computer-Aided Civil and Infrastructure Engineering*, 36(8), 962–977. doi: 10.1111/mice.12685
- Oulhen, E., Kolodziejczyk, N., Tandeo, P., Blanke, B., & Sévellec, F. (2024). Reconstructing the ocean state using argo data and a data-driven method. *Journal of Atmospheric*

and *Oceanic Technology*.

- Quemener, E., & Corvellec, M. (2013). SIDUS—the Solution for Extreme Deduplication of an Operating System. *Linux J.*, 2013(235).
- Raissi, M., Perdikaris, P., & Karniadakis, G. (2019). Physics-informed neural networks: A deep learning framework for solving forward and inverse problems involving nonlinear partial differential equations. *Journal of Computational Physics*, 378, 686-707.
- Sitzmann, V., Martel, J., Bergman, A., Lindell, D., & Wetzstein, G. (2020). Implicit neural representations with periodic activation functions. *Advances in Neural Information Processing Systems*, 33, 7462–7473.
- Sonneveld, M., Lguensat, R., Jones, D. C., Dueben, P. D., Brajard, J., & Balaji, V. (2021). Bridging observations, theory and numerical simulation of the ocean using machine learning. *Environmental Research Letters*, 16(7), 073008.
- Vallis, G. K. (2017). *Atmospheric and oceanic fluid dynamics*. Cambridge University Press.
- Venaille, A. (2012). Bottom-trapped currents as statistical equilibrium states above topographic anomalies. *Journal of Fluid Mechanics*, 699, 500–510.
- Wang, Y., Sun, J., Bai, J., Anitescu, C., Eshaghi, M. S., Zhuang, X., ... Liu, Y. (2024). Kolmogorov arnold informed neural network: A physics-informed deep learning framework for solving pdes based on kolmogorov arnold networks. *arXiv preprint arXiv:2406.11045*.
- Wong, A. P., Wijffels, S. E., Riser, S. C., Pouliquen, S., Hosoda, S., Roemmich, D., ... others (2020). Argo data 1999–2019: Two million temperature-salinity profiles and subsurface velocity observations from a global array of profiling floats. *Frontiers in Marine Science*, 7, 700.
- Yoon, S., Park, Y., Gerstoft, P., & Seong, W. (2024). Predicting ocean pressure field with a physics-informed neural network. *The Journal of the Acoustical Society of America*, 155(3), 2037–2049.
- Zhu, L., Jiang, X., Lefauve, A., Kerswell, R. R., & Linden, P. (2024). New insights into experimental stratified flows obtained through physics-informed neural networks. *Journal of Fluid Mechanics*, 981, R1.